ELSEVIER

Contents lists available at ScienceDirect

Materials Science & Engineering A

journal homepage: www.elsevier.com/locate/msea



Microporosity and statistical size effect on the fatigue strength of cast aluminium alloys EN AC-45500 and 46200



Martin Leitner^{a,*}, Christian Garb^b, Heikki Remes^c, Michael Stoschka^a

- a Christian Doppler Laboratory for Manufacturing Process based Component Design, Montanuniversität Leoben, Chair of Mechanical Engineering, Leoben, Austria
- ^b Montanuniversität Leoben, Chair of Mechanical Engineering, Leoben, Austria
- ^c Aalto University, Department of Mechanical Engineering, Espoo, Finland

ARTICLE INFO

Keywords: Fatigue strength Cast aluminium alloy Microporosity Extreme value distribution Statistical size effect X-ray tomography

ABSTRACT

This paper investigates the fatigue strength of two cast aluminium alloys, EN AC-45500 and 46200, dealing with the influence of microporosity and the statistical size effect. Small-scale round specimens are extracted from cylinder heads and crank cases as typical cast components in automotive industry. Uniaxial fatigue tests under alternating tension/compression loading are performed. Local microstructural properties, such as second dendrite arm spacing and microporosity, are characterized by means of metallography, fracture surface analysis utilizing scanning electron microscopy, and X-ray computed tomography. The measurements reveal significant differences in microporosity and microstructure depending on the extraction position and specimen type. These findings are reflected by the experimental test results showing that the microporosity majorly affects the fatigue behaviour with a maximum difference in fatigue resistance at ten million load-cycles of up to 39% in case of the EN AC-45500 specimens. Additional experiments involving two different EN AC-46200 specimen types exhibiting unequal highly-stressed volumes demonstrate a reduction of the high-cycle fatigue strength by 8% caused by the statistical size effect. Fatigue strength assessment incorporates the application of the model by Tiryakioğlu based on the extreme value distribution of the micropore sizes by Gumbel, as well as the √area approach by Murakami. The evaluated results agree well to the fatigue tests enabling a local fatigue strength assessment under consideration of manufacturing process dependent material characteristics.

1. Introduction

Casted Al-Si-Mg alloys are widely utilized for high-performance, lightweight parts within mobility sectors [1], and especially in automotive industry [2] due to their advantageous castability and comparably beneficial strength to weight ratio. Although advanced casting technologies [3] are facilitated, the resulting microstructural and mechanical material properties strongly depend on casting process parameters as well as specific material compositions [4]. Such material discontinuities strongly affect the fatigue life of cyclically-loaded parts causing failure by microporosity-induced defects [5–7] and microstructural inhomogeneities [8–10]. Focus of this work is laid on the effect by micropores as primary influence factor on the fatigue strength of casted Al-Si-Mg alloys [11] utilized in complexly-shaped lightweight automotive components, such as internal combustion engine EN AC-45500 cylinder heads and EN AC-46200 crank cases, see Fig. 1.

A study in [12] investigating Al-Si cast alloys concludes that variations in fatigue strength may be obtained even by testing an increased number of specimens, which is mainly caused by the statistically

distributed occurrence of micropores. Hence, a comparably huge number of samples are essential to obtain a meaningful mean value and scatter index of manufacturing process dependent fatigue strength characteristics. Such a testing scheme is basically a rather time-consuming and expensive process. In order to cover the statistical distribution of casting defects, an incorporation of Weibull statistics [13] and microstructural parameters [14] within the fatigue analysis of Al-Si cast alloys is suggested in [12]. Furthermore, a weakest link concept based on a Weibull distribution function in [15] concludes that the fatigue strength distribution of weak links is different from the micropore size distribution, though fatigue crack initiation is predominantly associated with pores. Another work [16] presents that a log-normal distribution model may act as best fit to the statistical distribution of fatigue initiator sizes enabling a quantitatively correlation with the fatigue life of the experiments. However, a comparison of different statistical distributions for fatigue strength assessment is provided in [17]. Among them, one well suitable model for Al-castings [18] is based on an extreme value distribution of the micropore sizes introduced by Gumbel [19]. Thereby, the cumulative probability P for a certain

E-mail address: martin.leitner@unileoben.ac.at (M. Leitner).

^{*} Corresponding author.

Nomen	clature	N_{T}	number of load-cycles at transition knee point of S/N-
			curve
area	projected area of micropore	P	cumulative probability
B, m_1	parameters of fatigue life model by Tiryakioğlu	P_{f}	probability of failure
C_0, k_0	constants for crack initiation model	P_S	probability of survival
C_1, C_2, I	n ₂ parameters of fatigue approach by Murakami	R	stress ratio
DAS	second dendrite arm spacing	T_S	stress-based scatter index
d_{equ}	equivalent defect diameter	UTS	ultimate tensile strength
HV	Vicker's Hardness	V	highly-stressed volume
k	constant for crack initiation model and Weibull parameter	α, β	constants for crack initiation model
k_1, k_2	slopes of S/N-curve	δ	scale parameter of extreme value distribution
k_{σ}	stress concentration factor at micropore	$\varepsilon_{ m equ}^{\ \ p}$	equivalent plastic strain
N	number of load-cycles until burst fracture	σ_{a}	nominal stress amplitude
N_{i}	number of load-cycles until crack initiation	σ_{R}	alternating fatigue resistance at ten million load-cycles
		λ	location parameter of extreme value distribution

equivalent defect diameter d_{equ} is given in Eq. (1) involving a micropore size distribution depended location λ and scale parameter δ .

$$P(d_{equ}) = \exp\left[-\exp\left(\frac{d_{equ} - \lambda}{\delta}\right)\right]$$
(1)

A study in [20] investigating the relationship between defect size and fatigue life distributions of Al-Si castings based on numerous experimental data sets shows that the equivalent diameter d_{equ} is well suited to statistically analyze fatigue-initiating defects. It equals the diameter of a circle, which features the same area as the corresponding defect, see Eq. (2).

$$d_{equ} = \sqrt{\frac{4 \cdot area}{\pi}} \tag{2}$$

Fig. 2 represents a typical crack-initiating shrinkage pore at a scanning-electron-microscopy (SEM)-analyzed fracture surface of a tested EN AC-46200 specimen as well as the corresponding depiction of

the area-value. In addition to this method, micropore sizes can be characterized on the basis of X-ray computed tomography and metallography [21]. Especially X-ray computed tomography, as non-destructive technique, experiences an increasing practicability due to developments regarding scan quality, such as improved resolution to properly measure complexly-shaped shrinkage pores, and efficiency [22]. Applying such elaborated methods facilitates a fatigue strength assessment involving a three-dimensional evaluation of microporosity [23] and enables an enhanced damage tolerant design of casted components [24].

Based on the extreme value distribution by Gumbel [19], a fatigue model to assess the limit value of failure probability P_f for a certain lifetime until burst fracture N is presented by Tiryakioğlu [20], see Eq. (3).

$$P_f(N) = 1 - \exp\left(-\exp\left(\frac{\lambda}{\delta} - \frac{2}{\delta \cdot \sqrt{\pi}} \cdot \left(\frac{N - N_i}{B \cdot \sigma_a^{-m_1}}\right)^{\frac{2}{2 - m_1}}\right)\right)$$
(3)

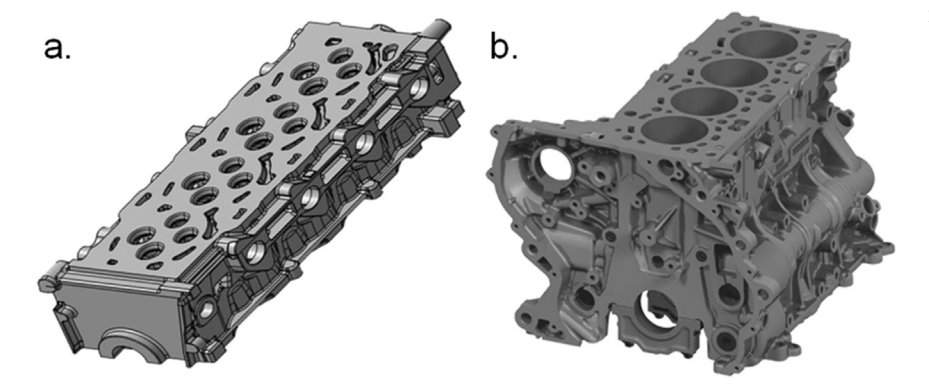
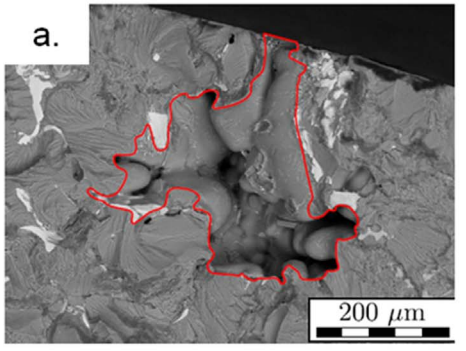


Fig. 1. Cylinder head manufactured of cast aluminium EN AC-45500 (a) and crank case made of EN AC-46200 (b).



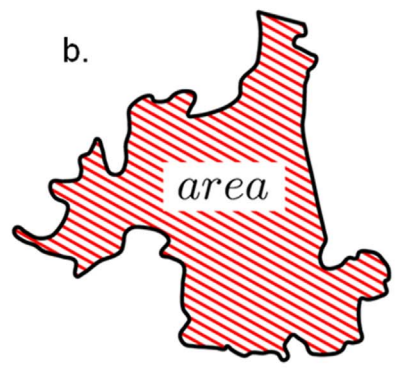


Fig. 2. SEM analysis of micropore at fractured surface of EN AC-46200 specimen (a) and evaluation of corresponding micropore area (b) according to [25].

Herein, λ and δ are the previously introduced parameters of the extreme value distribution, N_i is the lifetime until crack initiation, σ_a is the nominal stress amplitude, and B and m_1 are material dependent parameters. An experimental study for casted aluminium alloys in [26] reveals that the number of load-cycles until crack initiation N_i can exhibit values up to about 30–40% of the total lifetime N. In [27] a calculation procedure to estimate the crack initiation lifetime N_i based on a micro-cell model in [28] is presented. Herein, the stress amplitude σ_a is computed by the equivalent plastic strain ε_{equ}^P , a grain size dependent parameter k, and a constant β , see Eq. (4).

$$\sigma_a = k \cdot \varepsilon_{equ}^p \beta \tag{4}$$

The parameter k is evaluated on the basis of the second dendrite arm spacing *DAS* by a Hall-Petch [29,30] type relationship involving the constants k_0 and α , see Eq. (5).

$$k = k_0 + \frac{\alpha}{\sqrt{DAS}} \tag{5}$$

Further on, the fatigue life until crack initiation N_i can be determined by Eq. (6) involving the constant C_0 , whereby the crack initiation from a microcell is strongly influenced by the mechanism of local plastic strain accumulation [31,32].

$$N_{i} \cdot \varepsilon_{\ell q u}^{p} = C_{0} \cdot \frac{1}{DAS} \tag{6}$$

Combining Eqs. (4)–(6) leads to an estimation of the crack initiation lifetime N_i according to Eq. (7). As the local stress at the micropore is mostly fatigue-relevant, a supplementary stress concentration factor k_σ is multiplied with the nominal stress amplitude σ_a . Extensive numerical analyses in [33] show that k_σ depends on the specimen diameter, the equivalent pore size, and the pore location, and suggests simplified formulae to estimate this factor.

$$N_{i} = \frac{C_{0}}{DAS} \cdot \left(\frac{1}{k_{\sigma} \cdot \sigma_{a}} \cdot \left(k_{0} + \frac{\alpha}{\sqrt{DAS}} \right) \right)^{\frac{2}{\beta}}$$
(7)

An application of Eqs. (3) and (7) enables a fatigue life assessment in the finite life region incorporating the extreme value distribution of the micropore sizes as well as microstructural parameters, such as the second dendrite arm spacing. As not only the finite life, but also the high-cycle fatigue region is of great interest for a proper fatigue design, the \sqrt{area} model by Murakami [34] is additionally applied, see Eq. (8).

$$\sigma_R = C_1 \cdot \frac{(HV + C_2)}{(\sqrt{area})^{1/(2 \cdot m_2)}} \tag{8}$$

Herein, the alternating high-cycle fatigue resistance σ_R at a specified number of ten million load-cycles is affected by the Vicker's Hardness HV and the square root of the defect area \sqrt{area} , which is evaluated perpendicular to the principle load stress direction [35]. This method bases on the definition of a material-dependent threshold value of the linear-elastic stress intensity factor ΔK_{th} for small cracks, which is validated by numerous experimental data including steel and aluminium alloys in [36]. The constant C_1 bases on the defect location and can be defined as 1.43 for surface and 1.56 for subsurface cracks, and the constant C_2 as well as the exponent m_2 are material parameters [35]. A study in [37] shows the applicability of this method for a casted aluminium alloy and presents a method for the combination of poreclusters to one fatigue-effective defect. In the course of the micropore analysis within this paper, a common recommendation [38] is applied, which suggests a combination to a pore-cluster if single pores are less distant as the equivalent diameter of the smallest pore. Utilizing this recommendation and the √area concept, an assessment of the high-cycle fatigue strength is enabled. However, it is well known that for loadcycles above ten million, which is usually known as the very high-cycle fatigue region, a further decrease of the fatigue resistance may occur especially in case of defected materials, like aluminium castings

including microporosity or steels exhibiting defects like non-metallic inclusions [39].

Thereby, small fatigue crack initiation and crack growth [40] at the defects, which is majorly influenced by microstructural properties [41], need to be considered within the fatigue design. Fatigue strength characteristics are mostly evaluated experimentally on the basis of small-scale specimen, which may lead to differences in relation to a large-scale component [42]. In order to ensure a proper transfer of small-scale specimen results to large-scale aluminium cast structures, a consideration of size effects is of utmost importance [43]. Besides geometrical, technological, and surface-induced size effects, the socalled statistical size effect significantly influences the fatigue strength [44]. An overview of current state-of-the-art models to cover this effect for aluminium alloys is given in [45]. Among them, a comparably simple and feasible calculation method [46] based on the Weibull distribution [13] is capable to describe the fatigue resistance ratio of two components with different sizes $\sigma_{R,1}$ and $\sigma_{R,2}$ incorporating their corresponding highly-stressed volumes V_1 and V_2 by Eq. (9).

$$\frac{\sigma_{R,1}}{\sigma_{R,2}} = \left(\frac{V_2}{V_1}\right)^{\frac{1}{k}} \tag{9}$$

Herein, the parameter k acts as Weibull parameter and is defined as k = 10 for aluminium castings according to a common guideline [47]. It indicates that an increase of the highly-stressed volume leads to a decrease of the fatigue strength, which needs to be taken into account for an accurate fatigue design of large-scale components. This behaviour can be explained as the probability for an occurrence of extremely large defects increases for greater volumes and hence facilitating a reduction of the fatigue resistance according to the presented fatigue assessment concepts. As defect sizes majorly affect the fatigue strength of casted aluminium parts, one effective post-treatment method to enhance the fatigue resistance is hot isostatic pressing (HIP) [48]. Thereby, casting defects, such as shrinkage or gas pores, are distinctively reduced [49] leading to a significant increase of the fatigue behaviour [50]. Summarized, this paper investigates the fatigue strength of aluminium castings incorporating microporosity and statistical size effects. Fatigue tests with small-scale specimens manufactured of the cast aluminium alloys EN AC-45500 and 46200, which are commonly utilized for automotive lightweight components, are carried out. In addition, the effect of HIP on the fatigue strength is representatively shown for one selected test series. An extensive analysis of the micropore size distribution based on microscopical fracture surface analysis and X-ray computed tomography acts as basis for the fatigue assessment. In addition, focus is laid on the statistical size effect to ensure a proper transfer of small-scale specimen results to large-scale casted components.

2. Experimental work

2.1. Specimen geometries and manufacturing

The fatigue tests are conducted utilizing three different small-scale specimen types. For the investigation of the effect by the microporosity and HIP as post-treatment process, the round specimen geometry #1 shown in Fig. 3 is employed. The samples are extracted from casted

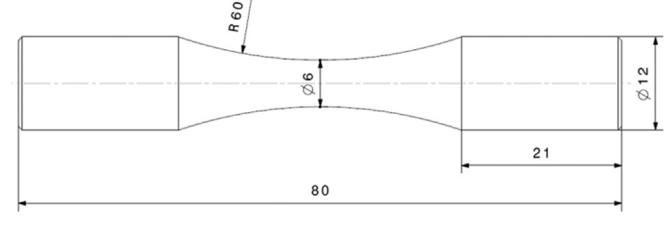


Fig. 3. Geometry of specimen #1 (EN AC-45500 and 46200).

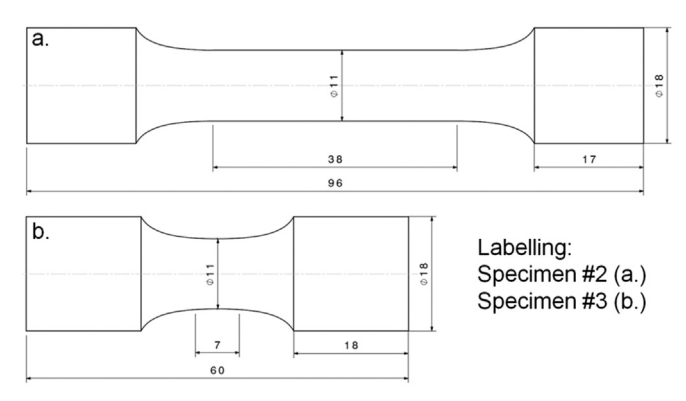


Fig. 4. Geometry specimen #2 (a) and #3 (b) (EN AC-46200).

aluminium alloy EN AC-45500 cylinder heads and EN AC-46200 crank cases with a T6 heat treatment at four different positions, denoted as position #1 to #4. Further information regarding the manufacturing procedure as well as material analysis is given in [51].

For the analysis of the statistical size effect, the round specimen geometries #2 and #3 are used, which are again manufactured from aluminium cast alloy EN AC-46200 crank cases, see Fig. 4. In order to examine the statistical size effect and not additional influences, only the length of the specimens is majorly different and the general shape at the clamping areas is kept similar.

A linear-elastic finite-element analysis at uniaxial tension loading incorporating hexahedral elements with quadratic shape functions is performed to evaluate the highly-stressed volumes of specimen type #2 and #3. The numerical results are depicted in Fig. 5 showing the distribution of the maximum principal stress. According to [52], the highly-stressed volume may be defined as value, which is loaded down to 90% of the peak stress. However, this value is common for steel components, but for aluminium castings exhibiting distinctive microporosity, a consideration of lower threshold values may be preferable as crack initiation can occur also within regions of reduced stresses. Hence, both highly-stressed volumes $V_{spec\#2}$ and $V_{spec\#3}$ are computed for a value of 60%, which is similar to a characteristic value given in [53], leading to a highly-stressed volume ratio of 2.58.

In order to ensure no additional affects by different microstructural properties an analysis of the secondary dendrite arm spacing *DAS* is performed. The normalized distribution as well as a representative microstructure of this crank case extraction position is presented in Fig. 6. The results indicate that the *DAS* is quite similar for both specimens with a minor deviation of 5%. Based on a calculation procedure in [54] it can be concluded that such a variation does not significantly affect the fatigue strength and therefore, the statistical size effect is predominantly investigated within this work.

Table 1

Mechanical and microstructural properties.

Material and extraction position	UTS	E	HV	DAS
	[MPa]	[MPa]	[HV]	[μm]
EN AC-45500 – Position #1 EN AC-45500 – Position #2 EN AC-45500 – Position #3 EN AC-46200 – Position #4	307 ± 10.6 290 ± 5.7	. ,	114 ± 3.3 117 ± 4.7	28 ± 6.6 56 ± 13.6 67 ± 13.1 31 ± 5.3

An overview of the mechanical properties, such as ultimate tensile strength UTS, Young's modulus E, and Vicker's hardness values HV as well as microstructural properties including the secondary dendrite arm spacing DAS for the investigated samples is provided in Table 1. For each test series a minimum number of three specimens are analyzed and a strain rate of $3.6\cdot10^{-3}$ mm/s is applied in the course of the quasi-static tensile tests. The relationship between UTS and HV correlates well to a suggestion given in [55] for casted Al-Si alloys.

2.2. Fatigue test results

2.2.1. Influence of extraction of position

At first, the effect of the specimen extraction position on the fatigue strength is experimentally investigated utilizing a resonance test rig with a testing frequency of about 70-100 Hz. Therefore, the presented specimen #1 is manufactured from casted aluminium alloy EN AC-45500 cylinder heads at the extraction positions #1 to #3. As the specimens are produced from different positions, the local microstructure incorporating different micropore size distributions is varying. An evaluation of these parameters on the basis of fracture surface analyses and X-ray computed tomography is subsequently presented. The results of the uniaxial tension/compression fatigue tests under fully reversed loading for a survival probability of $P_S = 50\%$ are shown in Fig. 7, whereby the values are normalized with the statistically evaluated high-cycle fatigue strength at ten million load-cycles of position #1. A statistical analysis based on the ASTM E 739 standard [56] is performed in the finite life region and utilizing the Arcsine VP-procedure [57] for the high-cycle fatigue regime. Above the fatigue life of the transition knee point N_T , a second slope $k_2 = 5 \cdot k_1$ is assumed in accordance to preliminary investigations with similar cast aluminium alloys in [58].

Table 2 summarizes the statistically evaluated S/N-curve parameters. The scattering is represented by the stress-based scatter index T_S , which equals the ratio of the high-cycle fatigue resistance σ_R at the survival probabilities of $P_S = 90\%$ to 10%. The results reveal a major effect on the fatigue strength characteristics due to the extraction

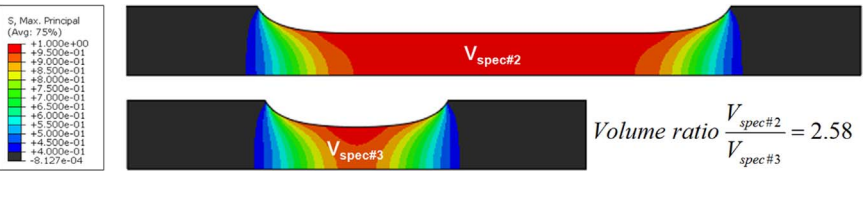


Fig. 5. Numerical analysis of highly-stressed volume V for specimen #2 and #3.

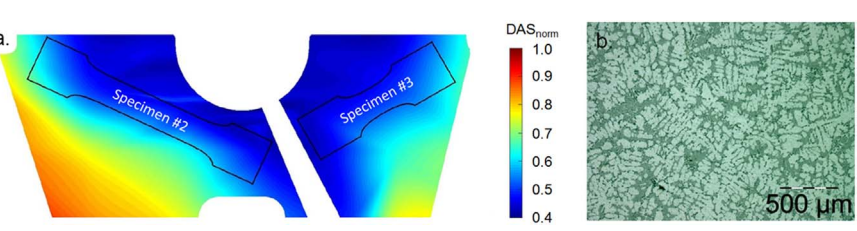


Fig. 6. Distribution of normalized secondary dendrite arm spacing *DAS*_{norm} (a) and representative sample of microstructure (b) according to [25].

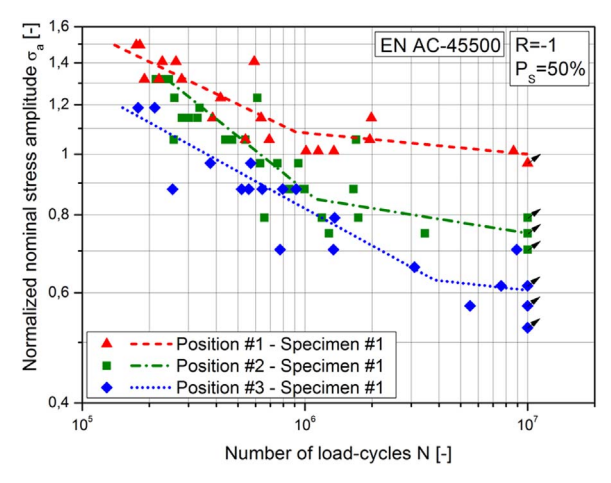


Fig. 7. S/N-curves of EN AC-45500 specimen #1 at positions #1 to #3.

Table 2 S/N-curve parameters of EN AC-45500 specimen #1 at positions #1 to #3.

Test series	σ _R	T _S	N _T	k ₁	k ₂
	[MPa]	[-]	[-]	[-]	[-]
Position #1	1.00	1:1.06	9.11e5	5.85	29.25
Position #2	0.75	1:1.15	1.12e6	3.52	17.60
Position #3	0.61	1:1.29	3.82e6	5.07	25.35

position. Thereby, the high-cycle fatigue resistance σ_R at ten million load-cycles shows a maximum difference of 39% between position #1 and #3. Furthermore, the number of load-cycles at the transition knee point N_T increases by a factor of over four for the same positions, which additionally diminishes the fatigue behaviour. The evaluated slopes k_1 and k_2 fit quite well to a suggestion in regard to component design and safety given in [59].

2.2.2. Statistical size effect

At second, the statistical size effect based on the presented geometries of casted aluminium alloy EN AC-46200 specimen geometry #2 and #3 is experimentally researched. Both specimen types are extracted from crank cases at position #4 and again tested under an alternating uniaxial tension/compression load. The resulting S/N-curves for a survival probability of $P_S = 50\%$ are depicted in Fig. 8, whereby all data points are normalized with the high-cycle fatigue strength of specimen #3 at ten million load-cycles. A comparison of the evaluated S/N-curve parameters in Table 3 maintains that the slopes k_1 and k_2 as well as the transition knee points N_T are similar for both testing conditions. However, in case of the fatigue resistance σ_R a decrease of 8% due to the increase of the highly-stressed volume for specimen #2 compared to type #3 is observed. As previously described, this decrease in fatigue strength can be majorly drawn to the statistical size effect, whereby a distinctive difference in regard to the micropore size distributions for both specimen geometries is subsequently presented.

2.2.3. Fatigue strength increase by HIP process

At third, the effect of HIP on the fatigue strength behaviour is investigated on the basis of EN AC-46200 specimen #1 extracted at crank case position #4. Fig. 9 depicts the fatigue test results before and after performing HIP as post-treatment process, whereat the data is normalized with the fatigue strength of the condition after HIP at ten million load-cycles.

The statistically analyzed S/N-curve parameters are summarized in Table 4. Thereby, a major increase of the high-cycle fatigue resistance σ_R by 31% is reached by the HIP process. In addition, the slopes k_1 and k_2 are raised by 78% and the transition knee point N_T elevates by almost

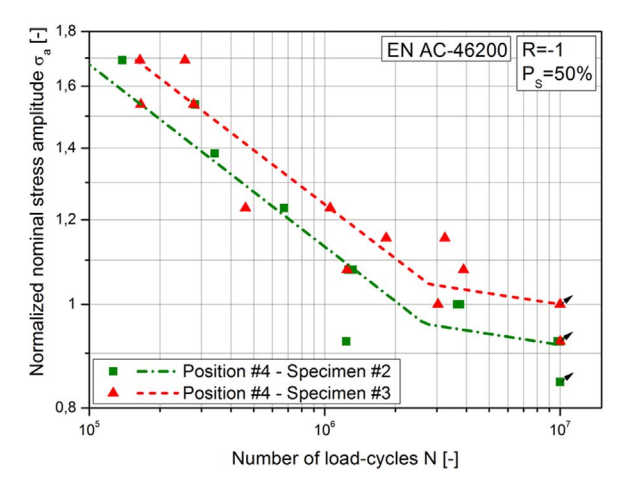


Fig. 8. S/N-curves of EN AC-46200 specimen #2 and #3 at position #4.

Table 3 S/N-curve parameters of EN AC-46200 specimen #2 and #3 at position #4.

Test series	σ _R	T _S	N _T	k ₁	k ₂
	[MPa]	[-]	[-]	[-]	[-]
Specimen #2	0.92	1:1.17	2.66e6	5.87	29.35
Specimen #3	1.00	1:1.16	2.77e6	6.05	30.25

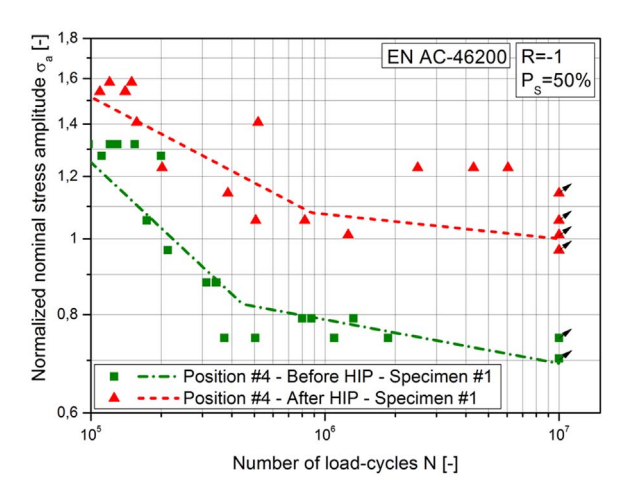


Fig. 9. S/N-curves of EN AC-46200 specimen #1 at position #4 before and after HIP.

Table 4
S/N-curve parameters of EN AC-46200 specimen #1 at position #4 before and after HIP.

Test series	σ _R	T _S	N _T	k ₁	k ₂
	[MPa]	[-]	[-]	[-]	[-]
Position #4 – Before HIP	0.69	1:1.10	4.45e5	3.58	17.90
Position #4 – After HIP	1.00	1:1.14	8.76e5	6.39	31.95

a factor of two. These beneficial effects are in accordance to the aforementioned studies [48,49] and confirm the effectiveness of this post-treatment technique.

2.3. Characterization of micropore size distribution

In order to perform a proper fatigue assessment of aluminium castings the knowledge of the micropore size distribution for each investigated aluminium alloy and extraction position is needed. The characterization can be performed destructively on the basis of fracture

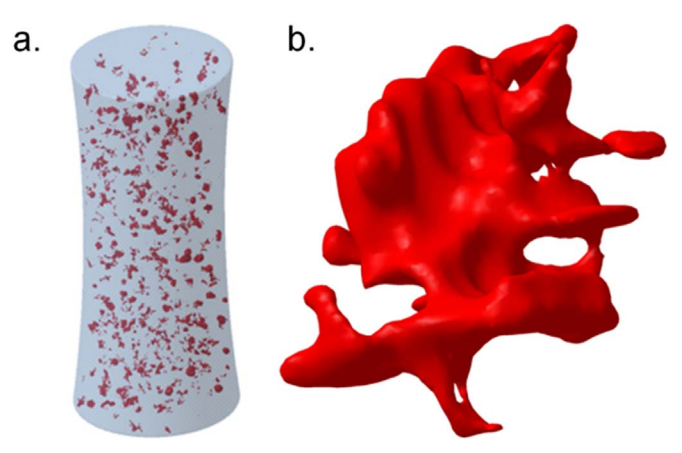


Fig. 10. X-ray tomography scan of EN AC-45500 specimen #1 (a) and representation of typical shrinkage pore (b).

surface analysis or non-destructively by X-ray computed tomography. Both methods are applied within this work and the results are used to evaluate the location λ and scale parameter δ of the extreme value distribution introduced by Gumbel [19]. A preliminary study [60] shows details in regard to X-ray computed tomography of the investigated specimens and validates the accuracy of this method. Fig. 10 demonstrates a X-ray tomography scan result of the highly-stressed mid-region of a EN AC-45500 specimen geometry #1 and a representation of a typical shrinkage pore exhibiting a maximum elongation of around 525 μm . For the analyzed specimens in this work, a scan resolution of 3 μm voxel size is utilized, which leads to a maximum scan volume of about 200 mm³. A voxel equals a value in three-dimensional space, which is located on a regular grid with a lattice size defining the resolution of X-ray computed tomography scans. A comparison of different scan resolutions is presented in [60].

In order to validate the results of the X-ray computed tomography scans, a fracture surface analysis by scanning electron microscopy is performed for each tested specimen. Fig. 11 shows a comparison of a shrinkage micropore analyzed by SEM at a fractured surface and the corresponding result of the X-ray tomography scan. In case of specimen #1 at extraction position #1 a maximum pore size of $48.8 \pm 26.6 \ \mu m$ is evaluated by the fracture surface analysis and a value of $52.4 \pm 30.6 \ \mu m$ in the course of the X-ray tomography scanning [51]. It shows that both methods agree quite well, which basically enables the applicability of non-destructive X-ray computed tomography scanning to properly evaluate micropore sizes.

Using the measured area of each micropore, the location λ and scale parameter δ of the Gumbel distribution [19] on the basis of the equivalent diameter d_{equ} as well as the $\vee area$ parameter for the application of the fatigue assessment model by Murakami [34] are defined. Additionally, the exponent m_1 to evaluate the fatigue behaviour on the basis of the method by Tiryakioğlu [20], as shown in Eq. (3), and m_2 for

 $200 \ \mu \mathrm{m}$

b.

Table 5
Parameters for fatigue assessment of EN AC-45500 specimen #1 at positions #1 to #3.

Test series	λ [μm]	δ [μm]	m ₁ [-]	√area [μm]	m ₂ [-]
Position #1	49.2	22.9	3.9	28.4	2.1
Position #2	72.9	21.5	2.8	59.3	
Position #3	170.8	39.6	4.7	143.8	

Table 6
Parameters for fatigue assessment of EN AC-46200 specimen #2 and #3 at position #4.

Test series	λ [μm]	δ [μm]	m ₁ [-]	√area [μm]	m ₂ [-]
Specimen #2 Specimen #3	195.1 184.1	94.9 64.1	4.1	161.4 253.7	3.0

the $\forall area$ model are evaluated by a best-fit approach. In the same way the incorporated material constants B and C_1 are appraised. The constant C_2 is defined as value for subsurface crack initiation according to [34]. The resulting parameters are summarized for the EN AC-45500 specimen #1 at the positions #1 to #3 in Table 5 and for the of EN AC-46200 specimen #2 and #3 at the position #4 in Table 6. These values are employed for the fatigue strength assessment in the subsequent section.

The aforementioned parameters are valid for the specimens without HIP as post-treatment involving preferential crack initiation at micropores. A detailed fracture surface analysis of the tested EN AC-46200 specimen #1 at position #4 after HIP indicates a distinctive change of the failure mechanism. The microporosity is significantly reduced due to the HIP process, thus leading to a crack initiation at other discontinuities within the material. Fig. 12 depicts two fractured surfaces of EN AC-46200 specimens after performing HIP as post-treatment process. It is clearly shown that the failure origin does not take place at a micropore, but occurs at other material inhomogeneities, such as Sior Fe-phases. This certain change of the failure mechanism is also observed in other studies investigating the effect of HIP on the fatigue strength of casted aluminium alloys, see [61,62]. However, as the focus of this paper is laid on the microporosity and its influence on the fatigue behaviour, the specimens tested in HIP condition are not considered in the following fatigue assessment. A fatigue design of casted aluminium components after HIP is set as prospective working topic.

3. Fatigue strength assessment

This section illustrates the fatigue strength assessment of the investigated specimens before HIP by the presented fatigue models involving the evaluated microstructural parameters. At first, the EN AC-45500 specimen #1 at the positions #1 to #3 are assessed. An application of the design model by Tiryakioğlu [20] at a normalized nominal stress amplitude of $\sigma_a=1.10$, which is located in the finite lifetime region for all three test series, is demonstrated in Fig. 13. Thereby, the

Fig. 11. SEM analysis of micropore at fractured surface of EN AC-45500 specimen (a) and corresponding result of X-ray tomography scan (b).

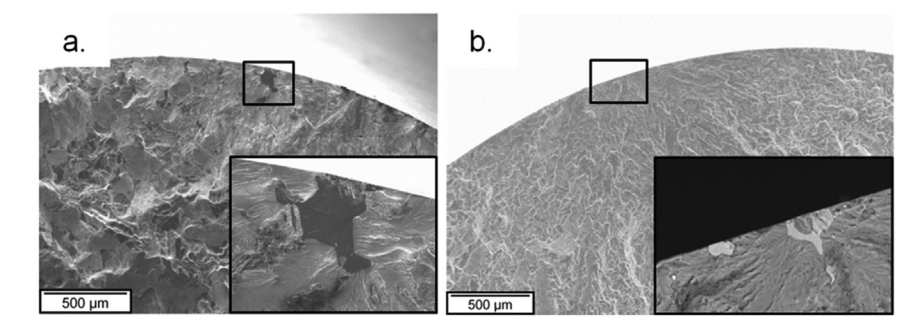


Fig. 12. SEM analysis of fractured surfaces of EN AC-46200 specimens after HIP with crack initiation at Si-phase (a) and at Fenhase (b)

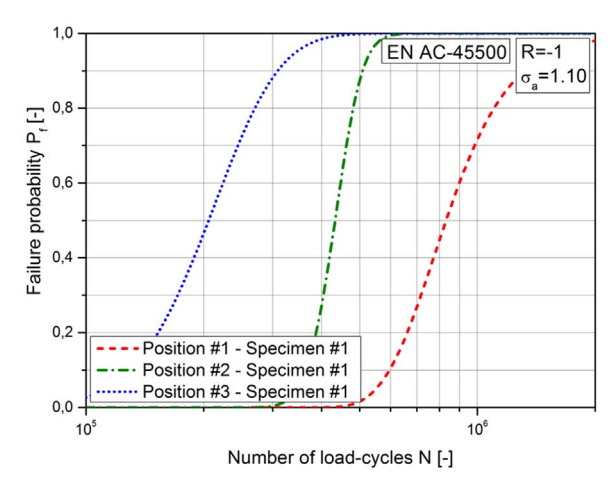


Fig. 13. Failure probability over load-cycles at a nominal stress amplitude of $\sigma_a=1.10$ of EN AC-45500 specimen #1 at positions #1 to #3.

Table 7
Fatigue assessment results of EN AC-45500 specimen #1 at positions #1 to #3.

Test series	Load-cycles $N_{\sigma a=1.10}$ [-]		Fatigue resista	nce σ _R [-]
	Experiment	Model [20]	Experiment	Model [34]
Position #1	845,000	835,000	1.00	0.86
Position #2	450,000	435,000	0.75	0.69
Position #3	225,000	205,000	0.61	0.58

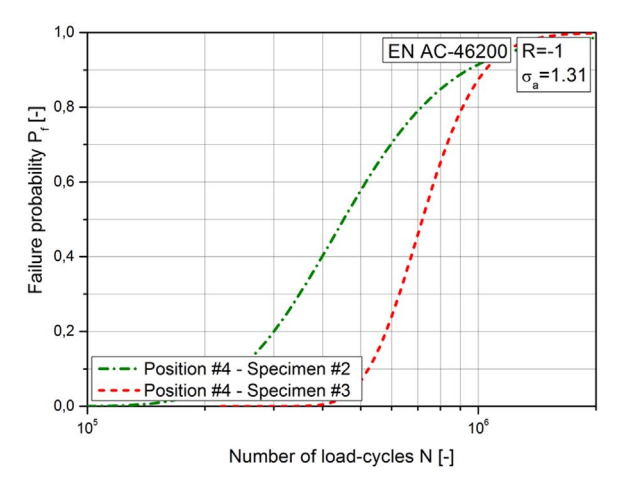


Fig. 14. Failure probability over load-cycles at a nominal stress amplitude of $\sigma_a=1.31$ of EN AC-46200 specimen #2 and #3 at position #4.

failure probability P_f over the number of load-cycles until burst fracture N is calculated in accordance to Eq. (3). Incorporating the approach given in [27] to estimate the crack initiation lifetime N_i it is shown that

Table 8
Fatigue assessment results of EN AC-46200 specimen #2 and #3 at position #4.

Test series	Load-cycles No	ra=1.31 [-]	Fatigue resistance σ_R [-]	
	Experiment	Model [20]	Experiment	Model [34]
Specimen #2 Specimen #3	430,000 745,000	450,000 720,000	0.92 1.00	0.93 0.99

in case of position #1, N_i is about 30% of the total lifetime, and for position #2 and #3, N_i is about zero. Herein, the parameters are defined as $k_0=103$, a=798, b=0.1, and $C_0=70.4$ in accordance to a similar cast aluminium alloy in [63]. Based on extensive numerical analyses in [34], the stress concentration factor at the pore is estimated towards a value of $k_\sigma=2.60$. The results crack initiation lifetime N_i are in sound accordance to [26] by specifying values of about 30–40% of the total lifetime N_i .

In addition to the fatigue assessment in the finite lifetime region, the presented \sqrt{area} model by Murakami [34] is applied to assess the fatigue resistance in the high-cycle fatigue regime at ten million load-cycles. A comparison of the results for the EN AC-45500 specimen #1 at the positions #1 to #3 by both models to the experimental fatigue strength values for a survival probability of $P_S=50\%$ is shown in Table 7. It is observed that the estimated numbers generally agree well to the fatigue test results. In case of the model by Tiryakioğlu [20], all fatigue life results N are conservatively underestimated with a maximum deviation of less than 9%. For the Murakami approach [34], again a conservative assessment of the fatigue resistance σ_R with a maximum deviation of 14% is detected.

At second, Fig. 14 depicts the results of the model by Tiryakioğlu [20] applied for the EN AC-46200 specimen #2 and #3 at position #4 at a normalized nominal stress amplitude of $\sigma_a = 1.31$. As both test series exhibit the same material properties, only the statistical size effect is investigated. Due to an increased highly-stressed volume in case of specimen #2 compared to type #3, additionally the location λ and scale parameter δ of the extreme value distribution based on the evaluated micropore sizes are enhancing. These values are reflected in the assessed failure probability P_f of both test series, whereby the specimen #3 demonstrates an enhanced fatigue life compared to specimen #2, which can be directly drawn to the statistical size effect. However, as both parameters λ and δ are increased, not only a shift of the distribution, but additionally a change of the shape occurs. Hence, an increase of the highly-stressed volume does not only affect the mean fatigue life, but ancillary enhances the scatter index, which can be also monitored at the fatigue test results.

A comparison of the results for the EN AC-46200 specimen #2 and #3 at the position #4 by both models to the experimental fatigue strength value at a survival probability of $P_S=50\%$ is shown in Table 8. Again both fatigue assessment concepts agree well to the experiments, where at the model by Tiryakioğlu [20] shows a minor overestimation by less than 5% for specimen #2 and a conservative underestimation by about 4% in case of specimen #3. For the

Murakami approach [34], a the fatigue resistance σ_R is overestimated by just 1% for specimen #2 and underestimated by only 1% in case of specimen #3. Summarized, an application of both models incorporating the evaluated parameters of the extreme value distribution by Gumbel [19] is able to properly cover the statistical size effect.

As introduced, another feasible approach [46] to assess the statistical size effect based on the Weibull distribution [13] is presented in Eq. (9). Utilizing the numerically computed ratio of the highly-stressed volumes of 2.58 in combination with the recommended Weibull parameter for aluminium castings [47] of k = 10, a fatigue resistance ratio $\sigma_{R,spec\#2}/\sigma_{R,spec\#3}$ of 0.91 is estimated. This value is in sound agreement to the experimental results exhibiting a ratio of 0.92. Hence, also the more simplified approach [46] is sufficiently capable to estimate the statistical size effect. However, manufacturing conditions, such as casting parameters or component geometry, significantly affect the local microstructural properties, like the second dendrite arm spacing and the micropore size distribution. Therefore, an incorporation of these local characteristics within the presented elaborated fatigue assessment procedures is suggested, as such manufacturing process dependent effects may have a fundamental impact on the local fatigue strength of casted aluminium components. As within this study the mean fatigue strength of the fatigue test results acts for comparison, prospective work will focus on the evaluation of accurate design values for higher survival probabilities P_S . Therefore, additional fatigue tests incorporating majorly enhanced sample batch sizes are scheduled to achieve more statistically substantiated findings, which are properly applicable to mass production in the automotive industry [64]. In addition, further influences on the fatigue strength, such as multiaxiality [65], complex load scenarios including variations in stress ratio [66] or variable amplitude loading [67], or elevated temperatures [68] are defined as future topics in this field of research.

4. Conclusions

This paper investigates the fatigue strength of the cast aluminium alloys EN AC-45500 and 46200 incorporating the influence of microporosity and the statistical size effect. Fatigue tests under uniaxial tension/compression loading at an alternating stress ratio reveal that the microporosity majorly affects the fatigue behaviour with a maximum difference in fatigue resistance σ_R at ten million load-cycles of up to 39% in case of the EN AC-45500 specimens. This influence can be majorly drawn to the different extraction positions exhibiting varying microstructural properties, such as second dendrite arm spacing and micropore size distributions. An extensive analysis of the local microstructure by metallographic analysis, scanning electron microscopy of fractured surfaces as well as X-ray computed tomography proof these variations. The statistical size effect is investigated with two different EN AC-46200 specimen types manufactured from the same extraction position, but featuring a dissimilar specimen length, which primarily leads to an unequal highly-stressed volume. The uniaxial experiments demonstrate that the specimen type exhibiting an increased highlystressed volume shows a reduction in fatigue resistance σ_R at ten million load-cycles by 8%, which can be directly drawn to the statistical size effect. A concluding fatigue strength assessment based on the model by Tirvakioğlu [20] utilizing the extreme value distribution of the micropore sizes by Gumbel [19], and the √area approach by Murakami [34] is performed. The results highlight a sound accordance to the experiments enabling a local fatigue strength assessment, which incorporates manufacturing process dependent material characteristics.

Acknowledgements

The financial support by the Austrian Federal Ministry of Science, Research and Economy and the National Foundation for Research, Technology and Development as well as the Christian Doppler Research Association is gratefully acknowledged.

References

- C.M. Sonsino, Structural durability of cast aluminium gearbox housings of underground railway vehicles under variable amplitude loading, Int. J. Fatigue 27 (2005) 944–953
- [2] R. González, A. González, J. Talamantes-Silva, S. Valtierra, R. Mercado-Solís, N. Garza-Montes-de-Oca, R. Colás, Fatigue of an aluminium cast alloy used in the manufacture of automotive engine blocks, Int. J. Fatigue 54 (2013) 118–126.
- [3] A. Luo, A. Sachdev, Bob Powell, Advanced casting technologies for lightweight automotive applications, in: Proceedings of the 69th World Foundry Congress, 2016.
- [4] F. Grosselle, G. Timelli, F. Bonollo, Doe applied to microstructural and mechanical properties of Al–Si–Cu–Mg casting alloys for automotive applications, Mater. Sci. Eng. A 527 (2010) 3536–3545.
- [5] Y.X. Gao, J.Z. Yi, P.D. Lee, T.C. Lindley, The effect of porosity on the fatigue life of cast aluminium-silicon alloys, Fatigue Fract Eng. Mater. Struct. 27 (2004) 559–570.
- [6] J.-Y. Buffiere, S. Savelli, P.H. Jouneau, E. Maire, R. Fougeres, Experimental study of porosity and its relation to fatigue mechanisms of model Al–Si7–Mg0.3 cast Al alloys, Mater. Sci. Eng. A316 (2001) 115–126.
- [7] Q.G. Wang, D. Apelian, D.A. Lados, Fatigue behavior of A356-T6 aluminum cast alloys. Part I. Effect of casting defects, J. Light Met. 1 (2001) 73–84.
- [8] S. Siegfanz, A. Giertler, W. Michels, U. Krupp, Influence of the microstructure on the fatigue damage behaviour of the aluminium cast alloy AlSi7Mg0.3, Mater. Sci. Eng. A565 (2013) 21–26.
- [9] D.A. Lados, D. Apelian, P.E. Jones, J.F. Major, Microstructural mechanisms controlling fatigue crack growth in Al–Si–Mg cast alloys, Mater. Sci. Eng. A 468–470 (2007) 237–245.
- [10] Q.G. Wang, D. Apelian, D.A. Lados, Fatigue behavior of A356/357 aluminum cast alloys. Part II: effect of microstructural constituents, J. Light Met. 1 (2001) 85–97.
- [11] Q.G. Wang, C.J. Davidson, J.R. Griffiths, P.N. Crepeau, Oxide films, pores and the fatigue lives of cast aluminum alloys, Metall. Mater. Trans. B 37B (2006) 887–895.
- [12] D. Casellas, R. Perez, J.M. Prado, Fatigue variability in Al–Si cast alloys, Mater. Sci. Eng. A 398 (2005) 171–179.
- [13] W. Weibull, A statistical distribution function of wide applicability, J. Appl. Mech. 18 (1952) 293–297.
- [14] A. Wickberg, G. Gustafsson, L. Larsson, Microstructural effects on the fatigue properties of a cast Al7SiMg alloy, SAE Tech. Pap. 840121 (1984).
- [15] Y. Zhang, J. Xu, T. Zhai, Distributions of pore size and fatigue weak link strength in an A713 sand cast aluminum alloy, Mater. Sci. Eng. A 527 (2010) 3639–3644.
- [16] X. Zheng, H. Cui, C.C. Engler-Pinto Jr., X. Su, W. Wen, Statistical relationship between fatigue crack initiator size and fatigue life for a cast aluminium alloy, Mater. Sci. Eng. A 580 (2013) 71–76.
- [17] K. Wallin, Statistical aspects of fatigue life and endurance limit, Fatigue Fract Eng. Mater. Struct. 33 (2010) 333–344.
- [18] M. Tiryakioğlu, On the size distribution of fracture-initiating defects in Al- and Mgalloy castings, Mater. Sci. Eng. A 476 (2008) 174–177.
- [19] E.J. Gumbel, Statistics of extremes, Dover Books on Mathematics, Dover Publ., Mineola NY, 1. publication, 1958 edition, 2004.
- [20] M. Tiryakioğlu, Relationship between defect size and fatigue life distributions in Al-7 Pct Si-Mg alloy castings, Metall. Mater. Trans. A 40A (2009) 1623–1630.
- [21] G. Nicoletto, R. Konecná, S. Fintova, Characterization of microshrinkage casting defects of Al–Si alloys by X-ray computed tomography and metallography, Int. J. Fatigue 41 (2012) 39–46.
- [22] J. Kastner, B. Harrer, H.P. Degischer, High resolution cone beam X-ray computed tomography of 3D-microstructures of cast Al-alloys, Mater. Charact. 62 (2011) 99–107.
- [23] O. Caty, J.-Y. Buffiere, E. Maire, J. Adrien, 3D characterization of the influence of porosity on fatigue properties of a cast Al alloy, Adv. Eng. Mater. 13 (3) (2011) 194–198.
- [24] M. Shirani, G. Härkegård, Damage tolerant design of cast components based on defects detected by 3D X-ray computed tomography, Int. J. Fatigue 41 (2012) 188–198.
- [25] P. Pauer, Fatigue Strength Estimation for Minor Failure Probabilities Based on the Statistical Size Effect (Master thesis), Montanuniversität Leoben, 2016 (in German).
- [26] K. Shiozawya, Y. Tohda, S.-M. Sun, Crack initiation and small fatigue crack growth behaviour of squeeze-casr Al-Si aluminium alloys, Fatigue Fract. Eng. Mater. Struct. 20 (1997) 237–247.
- [27] J.Z. Yi, Y.X. Gao, P.D. Lee, T.C. Lindley, Microstructure-based fatigue life prediction for cast A356-T6 aluminum-silicon alloys, Metall. Mater. Trans. A 37B (2006) 301–311.
- [28] Y.X. Gao, J.Z. Yi, P.D. Lee, T.C. Lindley, A micro-cell model of the effect of microstructure and defects on fatigue resistance in cast aluminum alloys, Acta Mater. 52 (2004) 5435–5449.
- [29] E.O. Hall, The deformation and ageing of mild steel: III discussion of results, Proc. Phys. Soc. B64 (1951) 747–753.
- [30] N.J. Petch, The cleavage strength of polycrystals, J. Iron Steel Inst. Lond. 174 (1953) 25–28.
- [31] K. Tanaka, T.T. Mura, A dislocation model for fatigue crack initiation, J. Appl. Mech. 48 (1981) 97–103.
- [32] F. Alexandre, S. Deyber, A. Pineau, Modelling the optimum grain size on the low cycle fatigue life of a Ni based superalloy in the presence of two possible crack initiation sites, Scr. Mater. 50 (2004) 25–30.
- [33] Y.X. Gao, J.Z. Yi, P.D. Lee, T.C. Lindley, The effect of porosity on the fatigue life of cast aluminium-silicon alloys, Fatigue Fract. Eng. Mater. Struct. 27 (2004) 559–570.
- [34] Y. Murakami, Material defects as the basis of fatigue design, Int. J. Fatigue 41 (2012) 2–10.

- [35] Y. Murakami, Metal Fatigue: Effects of Small Defects and Nonmetallic Inclusions, Flsevier, UK. 2002.
- [36] Y. Murakami, M. Endo, Effects of Hardness and Crack Geometries on Kth of Small Cracks Emanating from Small Defects, Mechanical Engineering Publications, London, 1986, pp. 275–293.
- [37] A. Tajiri, T. Nozaki, Y. Uematsu, T. Kakiuchi, M. Nakajima, Y. Nakamura, H. Tanaka, Fatigue limit prediction of large scale cast aluminum alloy A356, Procedia Mater. Sci. 3 (2014) 924–929.
- [38] BDG-Richtlinie P202, Volumendefizite von Gussstücken aus Aluminium-Magnesium- und Zinkgusslegierungen, 2010 (in German).
- [39] B. Pyttel, D. Schwerdt, C. Berger, Very high cycle fatigue is there a fatigue limit? Int. J. Fatigue 33 (2011) 49–58.
- [40] S. Ishihara, A.J. McEvily, Analysis of short fatigue crack growth in cast aluminum alloys, Int. J. Fatigue 24 (2002) 1169–1174.
- [41] T.O. Mbuya, I. Sinclair, A.J. Moffat, P.A.S. Reed, Micromechanisms of fatigue crack growth in cast aluminium piston alloys, Int. J. Fatigue 42 (2012) 227–237.
- [42] M. Avalle, G. Belingardi, M.P. Cavatorta, R. Doglione, Casting defects and fatigue strength of a die cast aluminium alloy: a comparison between standard specimens and production components, Int. J. Fatigue 24 (2002) 1–9.
- [43] Q.G. Wang, M. Praud, A. Needleman, K.S. Kim, J.R. Griffiths, C.J. Davidson, C.H. Caceres, A.A. Benzerga, Size effects in aluminium alloy castings, Acta Mater. 58 (2010) 3006–3013.
- [44] I. Bazios, H.-J. Gudladt, The fatigue lifetime estimation in consideration of the statistical size effect as example for the AlMgSi0,7 alloy, Mater. Werkst. 34 (2004) 21–28.
- [45] T. Tomaszewski, J. Sempruch, T. Piątkowski, Verification of selected models of the size effect based on high-cycle fatigue testing on mini specimens made of EN AW-6063 aluminum alloy, J. Theor. Appl. Mech. 52 (2014) 883–894.
- [46] H. Friederich, B. Kaiser, K.H. Kloos, Anwendung der Fehlstellentheorie nach Weibull zur Berechnung des statistischen Größeneinflusses bei Dauerschwingbeanspruchung, Mater. Werkst. 29 (1998) 178–184 (in German).
- [47] FKM-guideline, Analytical Strength Assessment of Components in Mechanical Engineering, 6th edition, VDMA-Verlag, Frankfurt am Main, Germany, 2012.
- [48] L. Ceschini, A. Morri, G. Sambogna, The effect of hot isostatic pressing on the fatigue behaviour of sand-cast A356-T6 and A204-T6 aluminum alloys, J. Mater. Process. Technol. 204 (2008) 231–238.
- [49] G. Ran, J. Zhou, Q.G. Wang, The effect of hot isostatic pressing on the microstructure and tensile properties of an unmodified A356-T6 cast aluminum alloy, J. Alloy. Compd. 421 (2006) 80–86.
- [50] M.H. Lee, J.J. Kim, K.H. Kim, N.J. Kim, S. Lee, E.W. Lee, Effects of HIPping on highcycle fatigue properties of investment cast A356 aluminum alloys, Mater. Sci. Eng. A340 (2003) 123–129
- [51] C. Garb, M. Leitner, F. Grün, Fatigue strength assessment of AlSi7Cu0.5Mg T6W castings supported by computed tomography microporosity analysis, Procedia Eng. 160 (2016) 53–60.

- [52] C.M. Sonsino, Zur Bewertung des Schwingfestigkeitsverhaltens von Bauteilen mit Hilfe örtlicher Beanspruchungen, Konstruktion 45 (1993) 25–33 (in German).
- [53] A. Diemar, R. Thumser, J.W. Bergmann, Statistischer Größeneinfluss und Bauteilfestigkeit, MP Mater. 46 (2004) 16–21 (in German).
- [54] H. Stroppe, Calculation of the S-N curve for cast aluminium alloys based on static tensile test and dendrite arm spacing, Mater. Werkst. 40 (2009) 738–742 (in German)
- [55] L. Ceschini, Alessandro Morri, Andrea Morri, A. Gamberini, S. Messieri, Correlation between ultimate tensile strength and solidification microstructure for the sand cast A357 aluminium alloy, Mater. Des. 30 (2009) 4525–4531.
- [56] ASTM E739, Standard Practice for Statistical Analysis of Linear or Linearized Stress-Life (S-N) and Strain-Life (e-N) Fatigue Data, 1998.
- [57] D. Dengel, Arc sine P-transformation an effective tool for graphical and numerical evaluation of planned Wöhler-experiments, J. Mater. Technol. 8 (1975) 253–261 (in German).
- [58] H. Leitner, Simulation des Ermüdungsverhaltens von Aluminiumgusslegierungen (Doctoral thesis), Montanuniversität Leoben, 2001 (in German).
- [59] C.M. Sonsino, Course of SN-curves especially in the high-cycle fatigue regime with regard to component design and safety, Int. J. Fatigue 29 (2007) 2246–2258.
- [60] C. Garb, M. Leitner, M. Tauscher, M. Weidt, R. Brunner, Statistical analysis of micropore size distributions in Al-Si castings evaluated by X-ray computed tomography, Metall. Mater. Trans. A, (Submitted for publication).
- [61] J.T. Staley Jr, M. Tiryakioğlu, J. Campbell, The effect of hot isostatic pressing (hip) on the fatigue life of A206-T71 aluminum castings, Mater. Sci. Eng. A 465 (2007) 136–145.
- [62] T.O. Mbuya, I. Sinclair, A.J. Moffat, P.A.S. Reed, Analysis of fatigue crack initiation and S-N response of model cast aluminium piston alloys, Mater. Sci. Eng. A 528 (2011) 7331–7340.
- [63] J.Z. Yi, Y.X. Gao, P.D. Lee, T.C. Lindley, Effect of Fe-content on fatigue crack initiation and propagation in a cast aluminum-silicon alloy (A356–T6), Mater. Sci. Eng. A 386 (2004) 396–407.
- [64] L. Makkonen, R. Rabb, M. Tikanmäki, Size effect in fatigue based on the extreme value distribution of defects, Mater. Sci. Eng. A 594 (2014) 68–71.
- [65] V.-D. Le, F. Morel, D. Bellett, N. Saintier, P. Osmond, Multiaxial high cycle fatigue damage mechanisms associated with the different microstructural heterogeneities of cast aluminium alloys, Mater. Sci. Eng. A 649 (2016) 426–440.
- [66] I. Koutiri, D. Bellett, F. Morel, L. Augustins, J. Adrien, High cycle fatigue damage mechanisms in cast aluminium subject to complex loads, Int. J. Fatigue 47 (2013) 44–57.
- [67] A.A. Dabayeh, R.X. Xu, B.P. Du, T.H. Topper, Fatigue of cast aluminium alloys under constant and variable-amplitude loading, Int. J. Fatigue 18 (1996) 95–104.
- [68] X. Zhu, J.W. Jones, J.E. Allison, Effect of frequency, environment, and temperature on fatigue behavior of E319 cast aluminum alloy: stress-controlled fatigue life response, Metall. Mater. Trans. A 39B (2008) 2681–2688.